





Article

Oscillatoria limnetica Mediated Green Synthesis of Iron Oxide (Fe₂O₃) Nanoparticles and Their Diverse In Vitro Bioactivities

Muhammad Haris ¹, Namra Fatima ¹, Javed Iqbal ^{2,*}, Wadie Chalgham ³, Abdul Samad Mumtaz ^{1,*}, Mohamed A. El-Sheikh ⁴ and Maryam Tavafoghi ⁵

¹ Department of Plant Sciences, Faculty of Biological Sciences, Quaid-i-Azam University, Islamabad 45320, Pakistan

² Department of Botany, Bacha Khan University, Charsadda 24420, Pakistan

³ Department of Mechanical and Aerospace Engineering, University of California, Los Angeles, CA 90095, USA

⁴ Botany and Microbiology Department, College of Science, King Saud University, Riyadh 11451, Saudi Arabia

⁵ Department of Bioengineering, University of California, Los Angeles, 410 Westwood Plaza, Los Angeles, CA 90095, USA

* Correspondence: javed89qau@gmail.com (J.I.); asmumtaz@qau.edu.pk (A.S.M.)

Abstract: Iron oxide nanoparticles (Fe₂O₃-NPs) were synthesized using *Oscillatoria limnetica* extract as strong reducing and capping agents. The synthesized iron oxide nanoparticles IONPs were characterized by UV-visible spectroscopy, Fourier transform infrared (FTIR), X-ray diffractive analysis (XRD), scanning electron microscope (SEM), and Energy dispersive X-ray spectroscopy (EDX). IONPs synthesis was confirmed by UV-visible spectroscopy by observing the peak at 471 nm. Furthermore, different in vitro biological assays, which showed important therapeutic potentials, were performed. Antimicrobial assay of biosynthesized IONPs was performed against four different Gram-positive and Gram-negative bacterial strains. *E. coli* was found to be the least suspected strain (MIC: 35 µg/mL), and *B. subtilis* was found to be the most suspected strain (MIC: 14 µg/mL). The maximum antifungal assay was observed for *Aspergillus versicolor* (MIC: 27 µg/mL). The cytotoxic assay of IONPs was also studied using a brine shrimp cytotoxicity assay, and LD₅₀ value was reported as 47 µg/mL. In toxicological evaluation, IONPs was found to be biologically compatible to human RBCs (IC₅₀: >200 µg/mL). The antioxidant assay, DPPH 2,2-diphenyl-1-picrylhydrazyl was recorded at 73% for IONPs. In conclusion, IONPs revealed great biological potential and can be further recommended for in vitro and in vivo therapeutic purposes.

Keywords: *Oscillatoria limnetica*; (Fe₂O₃); green synthesis; characterizations; biological applications



Citation: Haris, M.; Fatima, N.; Iqbal, J.; Chalgham, W.; Mumtaz, A.S.; El-Sheikh, M.A.; Tavafoghi, M. *Oscillatoria limnetica* Mediated Green Synthesis of Iron Oxide (Fe₂O₃) Nanoparticles and Their Diverse In Vitro Bioactivities. *Molecules* **2023**, *28*, 2091. <https://doi.org/10.3390/molecules28052091>

Academic Editors: Tsz Him Chow and Henglei Jia

Received: 3 January 2023

Revised: 22 January 2023

Accepted: 25 January 2023

Published: 23 February 2023



Copyright: © 2023 by the authors. Licensee MDPI, Basel, Switzerland. This article is an open access article distributed under the terms and conditions of the Creative Commons Attribution (CC BY) license (<https://creativecommons.org/licenses/by/4.0/>).

1. Introduction

Nanotechnology is advantageous and is a widely growing branch of science that has gained the significant attention of the scientific community in the recent era of modern technology [1]. In the last few decades, nanotechnology has gained more attention due to its distinct size-related effect [2]. Metal nanoparticles range from 1 to 100 nm and show unique and fascinating properties such as physical, chemical, optical scattering, and biological properties [3,4]. Among the different nanoparticles, IONPs have gained more importance due to their multifunctional applications in different fields such as the food industry, biotechnology, tissue engineering, and environmental bioremediations [5,6]. Iron oxide NPs have important applications in the field of science for wastewater treatment, drug delivery, magnetic resonance imaging, etc. [7,8].

The NPs are synthesized by various methods including physical, chemical, and biological methods [9,10]. Nanoparticle synthesis through chemical and physical methods requires expensive equipment, uses toxic chemical substances, and has major environmental effects on both biotic and abiotic components of the ecosystem [11,12]. Nanoparticles possess promising potential and could be defined by their minute size, large surface area, and

various shapes [13]. Nanotechnology can produce and manipulate things on the atomic scale ranging from 1 to 100 nm [14]. Nanoparticles are considered more important by virtue of their large surface area to volume ratio, which is why they are used in different fields such as biotechnology, tissue engineering, medicine, cosmetics, engineering, electronics, environmental bioremediation, and materials science [15,16]. The biological method of NP synthesis is preferred over physical and chemical methods, as the biological method is ecofriendly, less expensive, pollutant free, biosafe, and biocompatible [6,17]. In addition, nanoparticles synthesized with the help of physical and chemical methods are not friendly to the environment as they use toxic chemical substances and expensive equipment [18–20].

Different species of algae such as green algae, diatoms, and cyanobacteria have also been used as biotemplates for the green synthesis of nanoparticles and are considered very important due to the presence of biologically active chemical compounds and secondary metabolites which function as strong reducing, stabilizing, and capping agents [21–23]. Among the different inorganic nanomaterials, IONPs have shown unique and fascinating properties with functional adaptability; these characteristics give them applications in cosmetics products, nonlinear optics, biosensors, fibers, antimicrobials, etc. [16,24,25]. Nanoscale IONPs are attracting the particular attention of the scientific community by virtue of their antimicrobial action against bacteria, fungi, and viruses in contrast with various other nanoparticles [26,27]. Some new studies explained the potential of IONPs for environmental remediation and for their ability to reduce environmental pollution [28,29].

Iron oxide exists in various forms such as magnetite (Fe_3O_4), hematite ($\alpha\text{-Fe}_2\text{O}_3$), and Maghemite ($\beta\text{-Fe}_2\text{O}_3$); of these forms, hematite is characterized by many significant properties [30]. Hematite of the n-type exists in different shapes such as wire, plate, and shuttle [31]. This is the first report of the synthesis of iron nanoparticles using algae from Pakistan. The aim of the current study was to establish an innovative protocol for green synthesis of hematite-phase IONPs using the algal extract of *Oscillatoria limnetica* as a strong capping and reducing agent without the addition of different reducing and capping agents as used in chemical approaches. Moreover, different characterization techniques such as UV-spectroscopy Fourier Transform Infrared Spectroscopy (FTIR), X-ray Diffractive Analysis (XRD), Energy Dispersive X-ray analysis (EDX), and Scanning Electron Microscopy (SEM) analysis were used to determine the physical and chemical properties of IONPs. Furthermore, different bioactivities were performed to investigate the biomedical potentials of synthesized IONPs.

2. Results and Discussion

2.1. Biosynthesis and Characterization of IONPs

Nanoparticle synthesis using algal extract has advantage over physical and chemical methods, since the later involve use of hazardous chemicals and require tedious time-consuming procedures. Earlier studies have shown that hazardous chemicals may get adsorb on the surface of nanoparticles during chemical synthesis, consequently cannot be used for biomedical applications [32]. The biosynthesis of iron NPs was explained for the first time using aqueous algal extract of *Oscillatoria limnetica*. The importance of this genus is well recognized. Recent phytochemical studies showed that algae are a rich source of proteins, carbohydrate, terpenoids and glycosides [33]. These chemicals play a significant role in the reduction, stabilization and capping of nanoparticles. Algae-mediated synthesis of nanoparticles start once the precursor salt $\text{FeCl}_3 \cdot 6\text{H}_2\text{O}$ was added into *Oscillatoria limnetica*-mediated extract. The change in color of the solution at 80 °C showed the formation of iron NPs. The change in color of algal extract is due to surface plasmon vibrations [34]. A precise biosynthesis mechanism is shown in Figure 1.

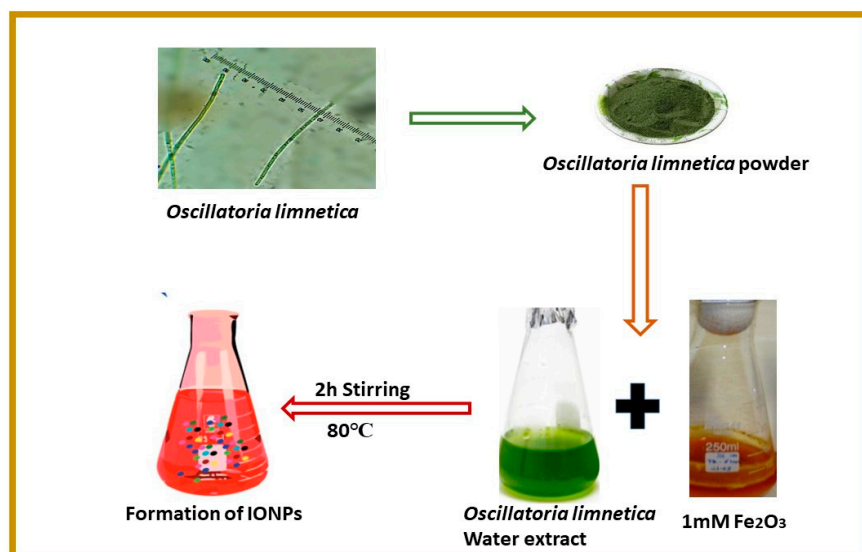


Figure 1. Novel protocol showing green synthesis of *Oscillatoria limnetica*-mediated IONPs.

2.2. UV-Visible Spectroscopy

IONP synthesis in aqueous solution was further confirmed by UV-visible spectroscopy, scanned at 350–600 nm. The highest absorbance peak was found at 471 nm. This highest absorbance peak revealed the synthesis of IONPs, which falls in the range of surface plasmon resonance of IONPs as shown in Figure 2. UV analysis plays a vital part in the characterization of iron NPs and can be used to obtain important information with regards to shape and size in addition to the stability of IONPs [35]. The results are matched with a previous report [7].

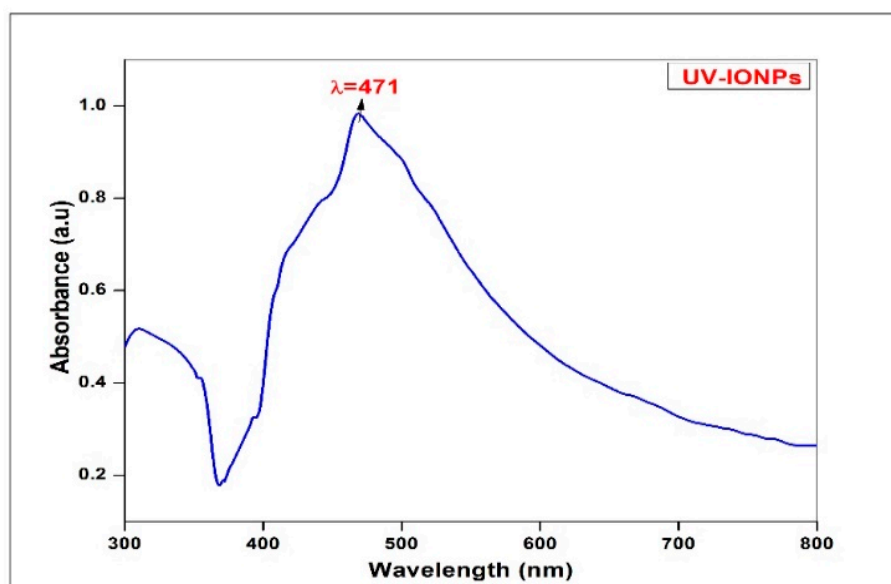


Figure 2. UV-visible spectra of *Oscillatoria limnetica*-mediated IONPs.

2.3. Fourier Transform Infrared Spectroscopy

The oscillation properties of biosynthesized iron NPs were evaluated using FTIR spectral analysis in the range of 500–4000 cm^{-1} . The results showed parallel regions for IR absorption. FTIR analysis plays a vital role in examining the functional groups of many organic and inorganic compounds. FTIR spectra show medium sharp peaks at 3781 cm^{-1} . The sharp bond at 3781 cm^{-1} is linked to the stretching vibration of the O-H bond. The peak at 3348 cm^{-1} depicted the N-H stretching of amine. The peak at 2326 cm^{-1} signified the

strong bond stretching of carbon dioxide ($\text{O}=\text{C}=\text{O}$). The peak at 1629 cm^{-1} was linked to weak bond stretching of alkene ($\text{C}=\text{C}$). The peak at 1440 cm^{-1} corresponded to the methyl group, with a medium bond stretching of alkane ($\text{C}-\text{H}$). Furthermore, the peak at 1010 cm^{-1} corresponded to carboxylic acid, $\text{O}-\text{H}$ stretching. The peaks lower than 1000 cm^{-1} showed a strong $\text{C}-\text{I}$ stretching with a halo groups, depicted different compounds adsorbed on the surface of nanoparticles, consequent to different functional groups present in *Oscillatoria limnetic* which stabilized the IONPs (Figure 3). The FTIR analysis results are consistent with an earlier study [36].

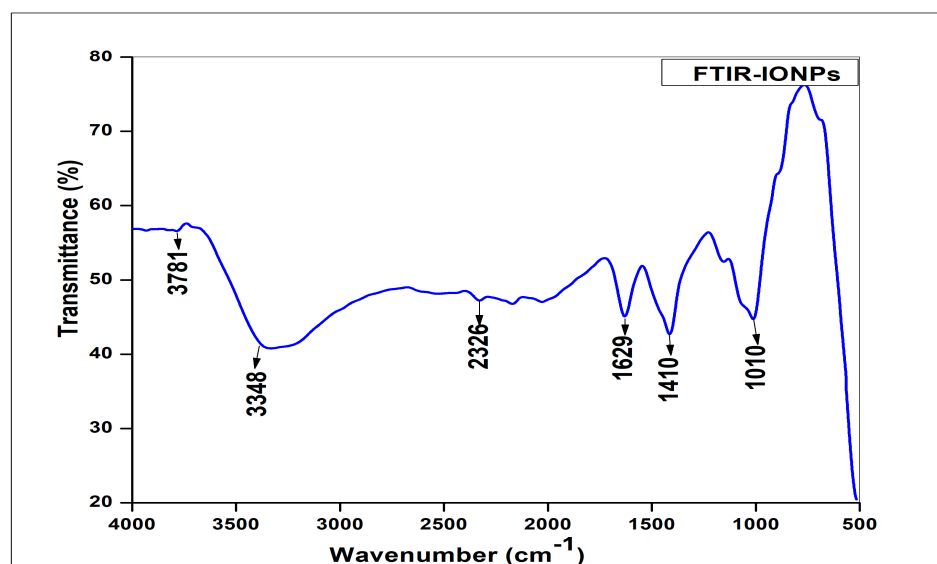


Figure 3. FTIR spectra showing different functional groups involved in the biosynthesis of IONPs.

2.4. X-ray Diffractive Analysis

X-ray powder diffraction (XRD) XRD spectrum has confirmed the single phase and formation of crystalline nature of iron oxide NPs. X-ray diffractive analysis has confirmed the development of iron NPs. The XRD spectrum explained that particles are in crystalline nature. The analyzed results showed that the shape of the crystalline was trigonal rhombohedral, and the size of the iron nanoparticles was obtained at a range of 23.33 nm using Debye Scherer equation. The 2θ size of the XRD pattern was in the range from 10° to 80° . There are different peaks of iron nanoparticles at 6.24° , 9.99° , 20.49° , 22.39° , 31.69° , 32.22° , 35.72° , 54.19° , 55.22° , 56.47° , and 75.14° which are Miller indexed to 100, 131, 400, 302, 123, 512, 110, 804, 530, 311, and 372. Bragg reflection of rhombohedral crystalline phase of iron NPs are shown in Figure 4. Some other peaks were also present in algal extract due to stabilizing agents as protein and enzyme [37]. The distinct analysis of XRD confirms the trigonal rhombohedral morphology of IONPs, which is confirmed through JCPD card No. 96-101-1241. The mean crystal size of IONPs was determined through different peaks from FWHMs, the average crystal size of iron nanoparticles was 23.33 nm, according to Scherer's equation as given, $D = K \lambda / \beta_{1/2} \cos \theta$. The results agreed with a previous report of [38].

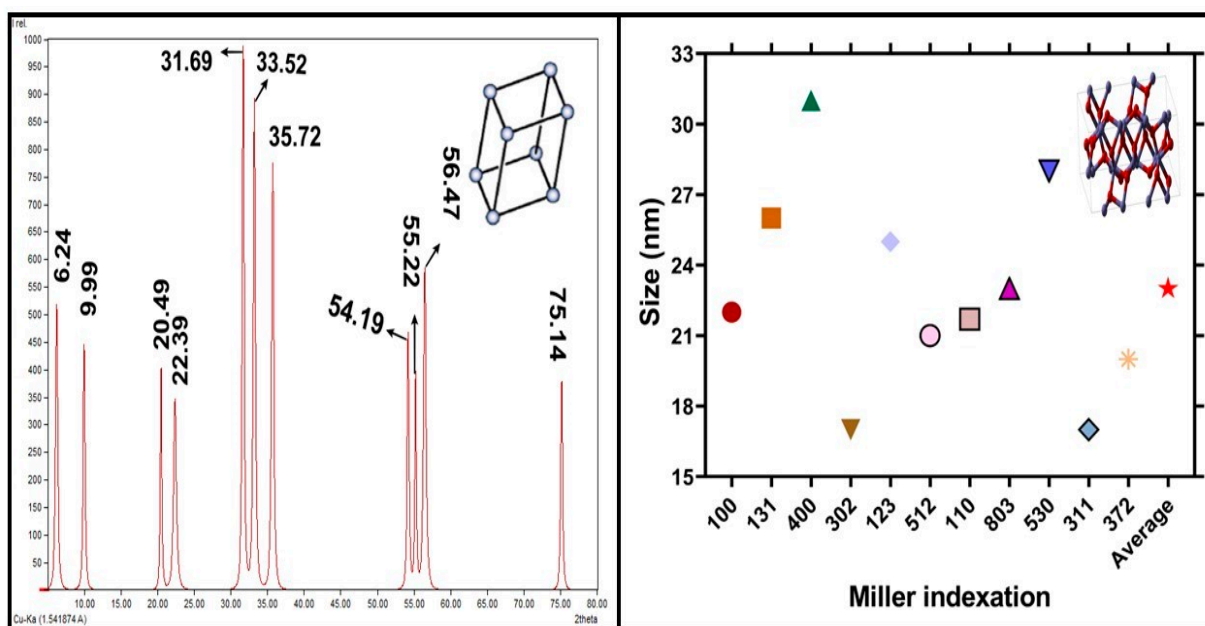


Figure 4. X-ray diffractive analysis of IONPs NPs. Size calculation via Scherer equation.

2.5. Scanning Electron Microscopy

The morphology of biosynthesized iron NPs was confirmed by scanning electron microscopy. Scanning electron microscopy was performed to identify the shape of biosynthesized IONPs (Figure 5), which confirm the formation of trigonal rhombohedral crystalline shapes in line with the XRD data. Large particles have gained specific shape due to crystal growth. SEM image of Fe_2O_3 -NPs showed that these NPs were present in contact with each other due to magnetic properties of IONPs [39,40]. Iron nanoparticles were characterized by SEM to ascertain the size and physical dimensions of the nanoparticles [41].

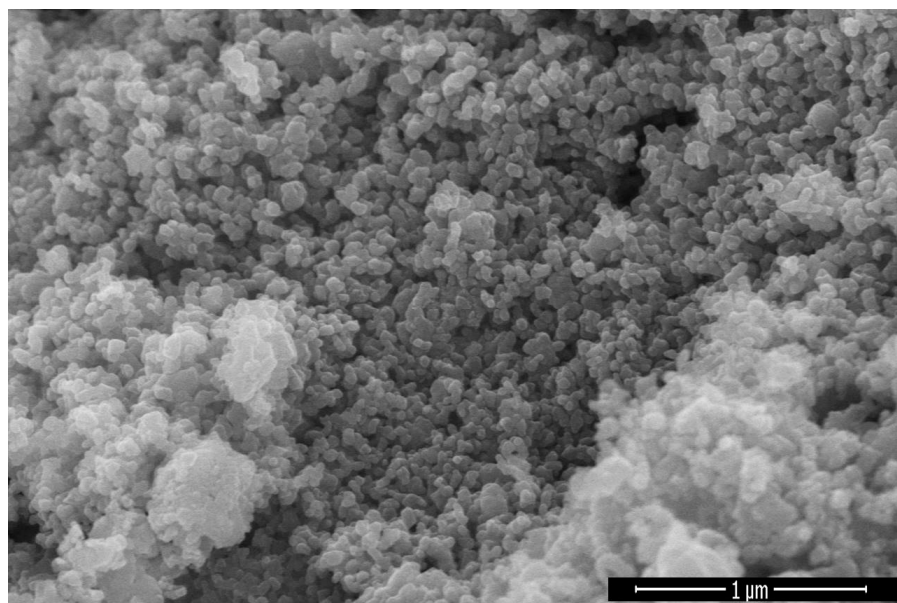


Figure 5. SEM image of *Oscillatoria limnetica*-mediated IONPs.

2.6. Energy Dispersive X-ray Analysis (EDX) Analysis

The elemental composition analysis showed that iron and oxygen were present in all samples. The occurrence of Iron (Fe) in elemental form was confirmed by energy-dispersive analysis X-ray spectra as depicted in the absorption peak visible in the range of 6–7 keV

(Figure 6). The EDX spectrum was obtained for the elemental composition which was present in iron nanoparticles. The occurrence of high peak of (Cl) and (O) show that the iron nanoparticle powder is in the chloride and oxide form. Due to surface plasmon resonance of iron nanoparticles, the absorbance peaks were present between 6 and 7 KeV. However, some other peaks and additional elements were also observed, namely Chlorine, Calcium, Oxygen, Sodium and Sulphur. Among other elements the occurrence of protein was also indicated [42]. However, in EDX spectra, (Fe) elements were observed with the highest percentage, which suggests that the major part was iron nanoparticles (Fe_2O_3). Hence, EDX analysis produced the qualitative and quantitative status of the Fe elements involved in the formation of IONPs [43].

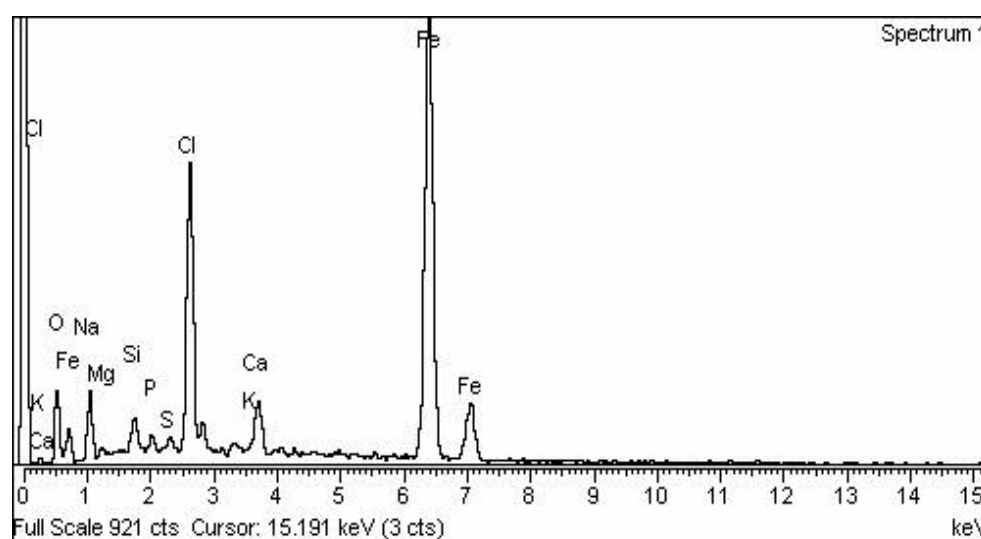


Figure 6. Energy-dispersive X-ray spectroscopy (EDX)EDX spectra showing the elemental composition of IONPs.

2.7. Antibacterial Assay

Antibacterial assay against different Gram-positive and Gram-negative strains were evaluated using the disc diffusion method. The Gram-positive strains that were utilized in current study were *S. aureus* and *B. subtilis*, whereas the Gram-negative strains were *E. coli* and *P. aeruginosa*. The antimicrobial mechanism of metal NPs against algae pathogens has been rarely studied [8], but the precise mechanism of action of NPs against microbes is not clear; however, different mechanism is involved. The antimicrobial assays of iron NPs are based on a loss of replication that disables the cellular protein and enzyme pathogen [44]. Different studies explain that NPs penetrate the cell membrane and cell wall and disrupt the cell integrity [45]. Some studies suggest NPs induced damage to protein, DNA, and RNA and finally cause cell death [46]. The most infectious diseases are due to bacteria that affect not only the mortality rate of the disease but also the costs of treatment [47]. More use of antibiotics causes different bacterial resistance problems, so scientists are working hard to develop new techniques to reduce the bacterial infections [48]. An antibacterial assay was performed for the following concentrations: 1 = 25 $\mu\text{g}/\text{mL}$, 2 = 50 $\mu\text{g}/\text{mL}$, 3 = 75 $\mu\text{g}/\text{mL}$, 4 = 100 $\mu\text{g}/\text{mL}$, 5 = 125 $\mu\text{g}/\text{mL}$, 6 = 150 $\mu\text{g}/\text{mL}$, and P = Ampicillin at 5 mg/mL. Our results reported that the antibacterial potential increased with increases in concentrations of NPs. Different strains were found to be susceptible to these nanoparticles. *P. aeruginosa* and *B. subtilis* were found to be more susceptible with MIC values of 10.7–14.4 $\mu\text{g}/\text{mL}$. *E. coli* and *S. aureus* were found to be the least effective with MIC values of 35–20 $\mu\text{g}/\text{mL}$. MIC values and ZOI are given in Table 1. In this study, the most successful antimicrobial assay was achieved at a higher concentration at 150 $\mu\text{g}/\text{mL}$ of IONPs, so it explains why effective antimicrobial activity was achieved at higher concentrations. The maximum inhibition of *S. aureus* had a range of 70 ± 0.03 at 150 $\mu\text{g}/\text{mL}$, *B. subtilis* had a range of 64.4 ± 0.03 at

150 $\mu\text{g}/\text{mL}$, *E. coli* had a range of 75 ± 0.03 at 150 $\mu\text{g}/\text{mL}$, and *P. aeruginosa* had a range of 42 ± 0.03 at 150 $\mu\text{g}/\text{mL}$. Different studies have been published to investigate the biogenic potential of nanoparticles [49]. An amount of 5 mg of the Ampicillin drug was taken as a positive control. No single concentration was found to be more effective than positive control Ampicillin. The antibacterial assay against different concentrations is shown in Figure 7. The results were confirmed by the previous report of [50].

Table 1. Zone of inhibition (ZOI) and Minimal inhibitory concentrations (MIC) calculations of different bacterial strains.

Compound	Concentrations	Zone of Inhibition (ZOI) and (% Inhibition)							
		Gram-Positive Bacteria				Gram-Negative Bacteria			
		<i>S. aureus</i>		<i>B. subtilis</i>		<i>E. coli</i>		<i>P. aeruginosa</i>	
	ZOI (mm)	(% Inhibition)	ZOI (mm)	(% Inhibition)	ZOI (mm)	(% Inhibition)	ZOI (mm)	(% Inhibition)	
IONPs	25 $\mu\text{g}/\text{mL}$	3 ± 0.03	20 ± 0.03	2.5 ± 0.03	14.4 ± 0.03	2 ± 0.03	35 ± 0.03	1.5 ± 0.03	10.7 ± 0.03
	50 $\mu\text{g}/\text{mL}$	4 ± 0.03	30 ± 0.03	2.7 ± 0.03	31.5 ± 0.03	2.5 ± 0.03	45 ± 0.03	2.3 ± 0.03	20.7 ± 0.03
	75 $\mu\text{g}/\text{mL}$	4.5 ± 0.03	35 ± 0.03	2.9 ± 0.03	34.5 ± 0.03	2.8 ± 0.03	51 ± 0.03	2.5 ± 0.03	23.2 ± 0.03
	100 $\mu\text{g}/\text{mL}$	5 ± 0.03	40 ± 0.03	3.5 ± 0.03	43 ± 0.03	3 ± 0.03	55 ± 0.03	2.7 ± 0.03	25.7 ± 0.03
	125 $\mu\text{g}/\text{mL}$	6 ± 0.03	50 ± 0.03	3.7 ± 0.03	45.8 ± 0.03	3.7 ± 0.03	69 ± 0.03	3 ± 0.03	29.5 ± 0.03
	150 $\mu\text{g}/\text{mL}$	8 ± 0.03	70 ± 0.03	5 ± 0.03	64.4 ± 0.03	4 ± 0.03	75 ± 0.03	4 ± 0.03	42 ± 0.03
Ampicillin	5 mg/mL	10 ± 0.05	100 ± 0.05	7 ± 0.05	100 ± 0.05	5 ± 0.05	100 ± 0.05	8 ± 0.05	100 ± 0.05
		Minimal inhibitory concentrations (MIC)							
		MIC ($\mu\text{g}/\text{mL}$)		MIC ($\mu\text{g}/\text{mL}$)		MIC ($\mu\text{g}/\text{mL}$)		MIC ($\mu\text{g}/\text{mL}$)	
IONPs		20 ± 0.03		14.4 ± 0.03		35 ± 0.03		10.7 ± 0.03	

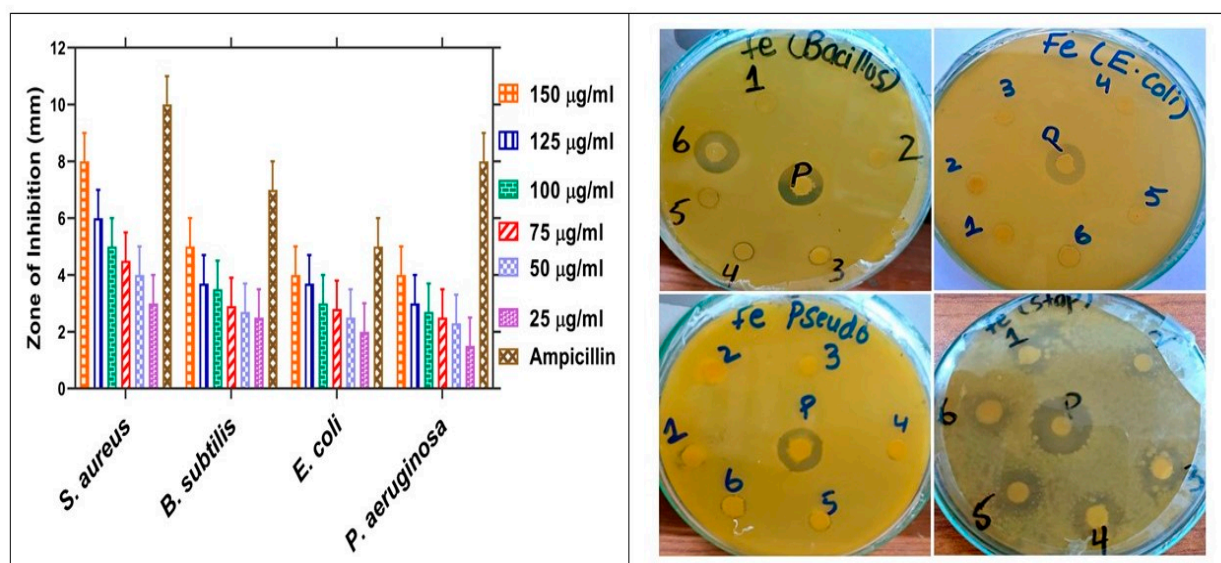


Figure 7. Antibacterial potential of *Oscillatoria limnetica*-mediated IONPs.

2.8. Antifungal Assay

To study the antifungal potential of biosynthesized IONPs, 30 mg of iron nanoparticles were dispersed in 30 mL of Dimethyl sulfoxide (DMSO) [41]. Various concentrations of IONPs and chemical fungicide (Fluconazole) showed variable growth inhibition (Figure 8 and Table 2). Antifungal assays of biosynthesized IONPs were evaluated against various fungal strains in the concentration range of 50–200 $\mu\text{g}/\text{mL}$. The different fungal strains used were *Rhizopus microsporus* and *Aspergillus versicolor*. Previously, iron NPs were shown to arrest the mycelial growth of *Rhizopus microsporus* and *Aspergillus versicolor* [51]. A recent report on the molecular level of *Rhizopus microsporus* and *Aspergillus versicolor* in response to iron NPs showed the generation of reactive oxygen species (ROS) [51]. Furthermore, the

application of iron NPs on tomato seedling has been shown to stimulate the antioxidant potential in hydroponics, which are considered to possibly increase the antimicrobial action of nanoparticles [27]. Increasing concentrations of iron nanoparticles showed positive effects on the growth of these two mycelia, and maximum % inhibition was observed at 200 $\mu\text{g}/\text{mL}$ of IONPs. Our results have shown that as we increase the concentration of IONP, there is an increase in the % inhibition and zone of inhibition. Formation of the zone around the well is directly proportional to NP concentrations. The maximum % inhibition of *Rhizopus microsporus* ranged from 47 ± 0.03 to 200 $\mu\text{g}/\text{mL}$, 40 ± 0.03 to 150 $\mu\text{g}/\text{mL}$, and *Aspergillus versicolor* ranged from 73 ± 650.03 to 200 $\mu\text{g}/\text{mL}$, 61 ± 0.03 to (150 $\mu\text{g}/\text{mL}$). *Aspergillus versicolor* was found to be maximally susceptible with an MIC value of (27 $\mu\text{g}/\text{mL}$). *Rhizopus microsporus* was found to be least susceptible with an MIC value of (53 $\mu\text{g}/\text{mL}$). Our study explains that iron NPs have a great potential effect on the formation of spore-producing fungi. The results are consistent with previous study of [52].

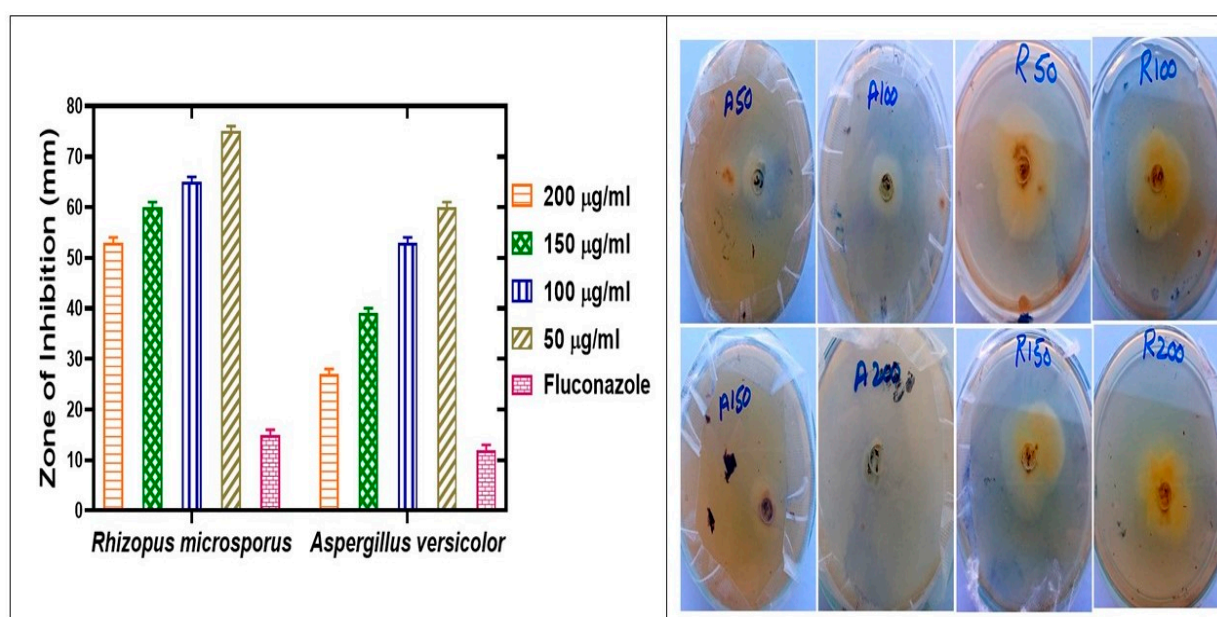


Figure 8. Antifungal potential of *Oscillatoria limnetica*-mediated IONPs.

Table 2. Zone of inhibition (ZOI) and minimum inhibitory concentration (MIC) ZOI and MIC calculation of fungal strains.

Compound	Concentrations	Zone of Inhibition (ZOI) and (% Inhibition)			
		Fungal Strains			
		<i>Rhizopus microsporus</i>		<i>Aspergillus versicolor</i>	
		ZOI (mm) and (% Inhibition)	ZOI (mm) and (% Inhibition)	ZOI (mm) and (% Inhibition)	ZOI (mm) and (% Inhibition)
IONPs	50 $\mu\text{g}/\text{mL}$	75 ± 0.03	25 ± 0.03	60 ± 0.03	40 ± 0.03
	100 $\mu\text{g}/\text{mL}$	65 ± 0.03	35 ± 0.03	53 ± 0.03	47 ± 0.03
	150 $\mu\text{g}/\text{mL}$	60 ± 0.03	40 ± 0.03	39 ± 0.03	61 ± 0.03
	200 $\mu\text{g}/\text{mL}$	53 ± 0.03	47 ± 0.03	27 ± 0.03	73 ± 0.03
(Fluconazole)	5 mg/mL	15 ± 0.05	100 ± 0	12 ± 0.05	100 ± 0
Minimal inhibitory concentrations (MIC)					
		MIC ($\mu\text{g}/\text{mL}$)		MIC ($\mu\text{g}/\text{mL}$)	
IONPs		53 ± 0.03		27 ± 0.03	

2.9. Antioxidant Assay

Biosynthesized IONPs have strong potential against antioxidant assay. There are different methods to measure antioxidant assay, but DPPH is most important assay for checking antioxidant potentials of nanoparticles. Antioxidant activities of iron nanoparticles were studied via DPPH assay. DPPH (1,1-diphenyl-2-pyridyl-hydrazine) free radicals were used to test the sample at different concentrations to determine their antioxidant potential [53]. The antioxidant activity of IONPs was studied at different concentrations ranging from 25 to 150 $\mu\text{g}/\text{mL}$. The maximum value of the antioxidant was $73 \pm 0.03\%$ at (150 $\mu\text{g}/\text{mL}$). The IONPs scavenged the DPPH free radical at different values of up to 73 ± 0.03 , 59 ± 0 , 51 ± 0.03 , 39.8 ± 0.03 , 41 ± 0.002 , and $24 \pm 0.003\%$ at concentrations of 150, 125, 100, 75, 50, and 25 $\mu\text{g}/\text{mL}$, respectively, as shown in Table 3. The antioxidant assay of IONPs is shown in Figure 9. The results explain that the higher the concentration, the higher the antioxidant activity will be. The results of the antioxidant activity decrease with a decrease in the concentrations of nanoparticles. Standard ascorbic acid was taken as a positive control. The IC_{50} values of all concentrations are shown in Table 3. The results are confirmed by a recent study by [54].

Table 3. IC_{50} and FRSA values calculations for antioxidant assay.

Concentration of NPs	% FRSA	IC_{50}
25 $\mu\text{g}/\text{mL}$	24 ± 0.003	1.32
50 $\mu\text{g}/\text{mL}$	37 ± 0.002	3.9
75 $\mu\text{g}/\text{mL}$	41.8 ± 0.03	6.4
100 $\mu\text{g}/\text{mL}$	51 ± 0.03	9.02
125 $\mu\text{g}/\text{mL}$	59 ± 0	11.6
150 $\mu\text{g}/\text{mL}$	73 ± 0.03	14.2

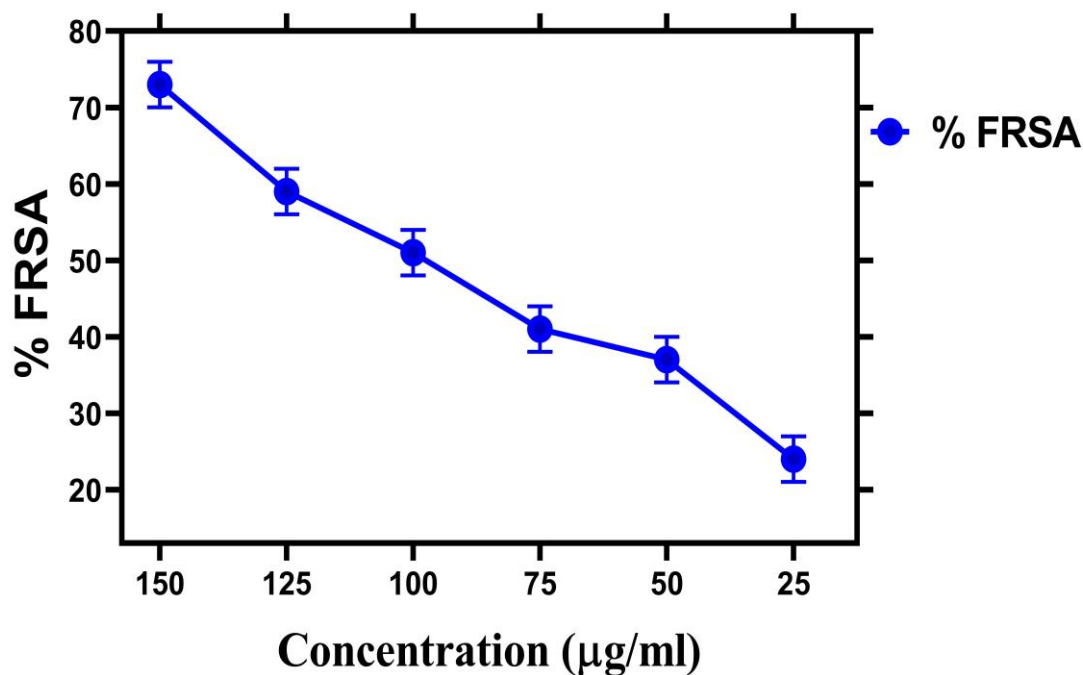


Figure 9. Antioxidant potential of a synthesized IONPs.

2.10. Hemolytic Assay

Biocompatibility against Human RBCs

The toxicological and biocompatible nature of iron nanoparticles was investigated against human RBCs, as shown in Figure 10. According to the American Society for materials and testing designation, the biological molecules which show hemolysis below <2% are non-hemolytic, substances which show hemolysis at 2–5% are lightly hemolytic, and substances which show hemolysis at greater than (>5%) are hemolytic [55]. To determine the degree of toxicity of human RBCs, hemolytic assay of iron nanoparticles was studied. The biocompatibility nature of iron nanoparticles was evaluated towards human RBCs by using hemolytic activity in the concentration range of 50 to 200 $\mu\text{g}/\text{mL}$. The concentration of 50 $\mu\text{g}/\text{mL}$ showed 7.1% hemolysis, concentration of 100 $\mu\text{g}/\text{mL}$ showed 11.3% hemolysis, and concentration of 150 $\mu\text{g}/\text{mL}$ showed 14.8% hemolysis. At a concentration of 200 $\mu\text{g}/\text{mL}$, the percentage of hemolysis is 21.5%, that is, it shows strong hemolysis potential. A higher concentration of the hemolytic assay was found in a higher concentration of 200 $\mu\text{g}/\text{mL}$ than in lower concentrations, which explains why IONPs released hemoglobin into blood plasma when they contacted the surface of RBCs cells [56]. The biocompatibility nature of iron nanoparticles was assessed against human RBCs from the group O⁺. The maximum and minimum hemolytic potential is shown in Table 4. PBS (phosphate buffer saline) was taken as a negative control. The NPs are considered hemolytic when they ruptured the RBCs, thus releasing hemoglobin. Concentrations lower than 50 $\mu\text{g}/\text{mL}$ could be non-hemolytic, so IONPs at lower concentrations against human RBCs confirm their biocompatibility and nontoxic nature. Thus, the results prove that higher concentrations of IONPs will lead to adverse health effects. The results agree with an earlier report [50].

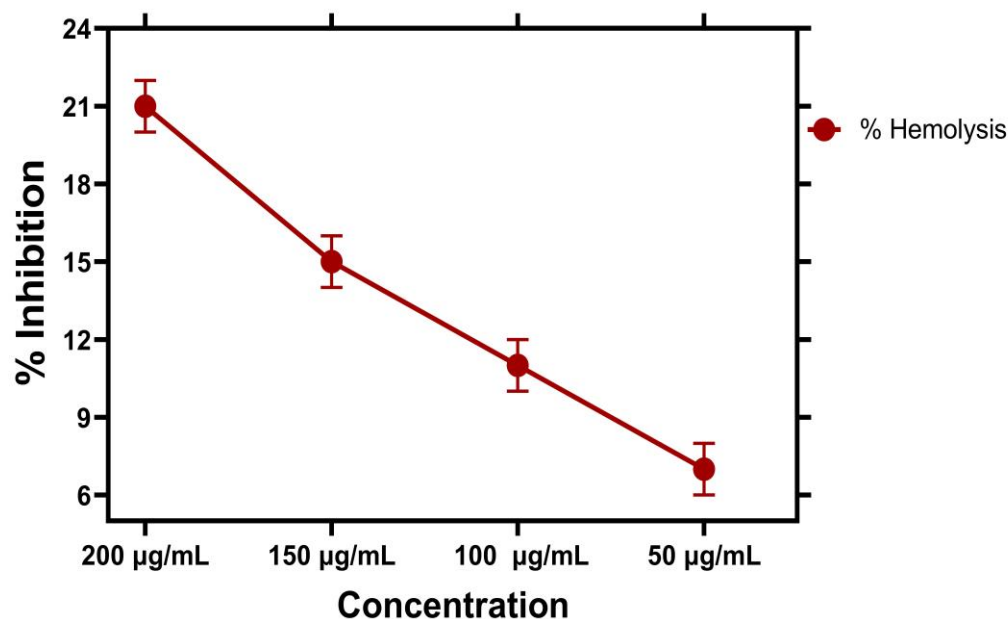


Figure 10. Biocompatibility potential of IONPs against human red blood cells RBC.

Table 4. IC₅₀ and hemolysis values for biocompatibility assay.

Concentrations of NPs	% Hemolysis	Triton X-100	IC ₅₀
50 $\mu\text{g}/\text{mL}$	7.1 \pm 0.003	0.200 \pm 0.40	49.5
100 $\mu\text{g}/\text{mL}$	11.3 \pm 0.005	0.62 \pm 0.90	99.5
150 $\mu\text{g}/\text{mL}$	14.8 \pm 0.006	0.79 \pm 0.01	149.5
200 $\mu\text{g}/\text{mL}$	21.5 \pm 0.003	0.180 \pm 0.20	199.5

2.11. Brine Shrimp Cytotoxicity Assay

Brine shrimp cytotoxicity (BSC) was ascertained to check the cytotoxic potential of IONPs against newly hatched eggs of *A. salina*. BSC is the most suitable test for confirming the potential of biological molecules. The cytotoxic assay of iron nanoparticles was established using *Artemia salina* [57]. It has been explained that the initial developmental stages of *Artemia* are greatly affected by toxins [58]. In the cytotoxicity assay, *Artemia salina* when tested with iron nanoparticles showed the best results as compared to algal extract. The brine shrimp cytotoxicity test is the most favorable cytotoxic screening test for confirming the potential of biological compounds. IONPs examined at four different concentrations (50 $\mu\text{g/mL}$, 100 $\mu\text{g/mL}$, 150 $\mu\text{g/mL}$, and 200 $\mu\text{g/mL}$) showed % mortality of IONPs at various concentrations (Figure 11). Maximum percentage mortality was found at 200 $\mu\text{g/mL}$ concentrations of iron nanoparticles. The median lethality dose LD_{50} was calculated as 47 $\mu\text{g/mL}$. Among various concentrations, 50 $\mu\text{g/mL}$ showed the best result with the lowest LD_{50} value. Hence, the BSC assay of IONPs showed a dose-dependent response. Our study explained that % mortality increased with increase in concentration of NPs. The highest concentration was more lethal compared to the lowest concentration [58]. The results are confirmed by a previous study [50].

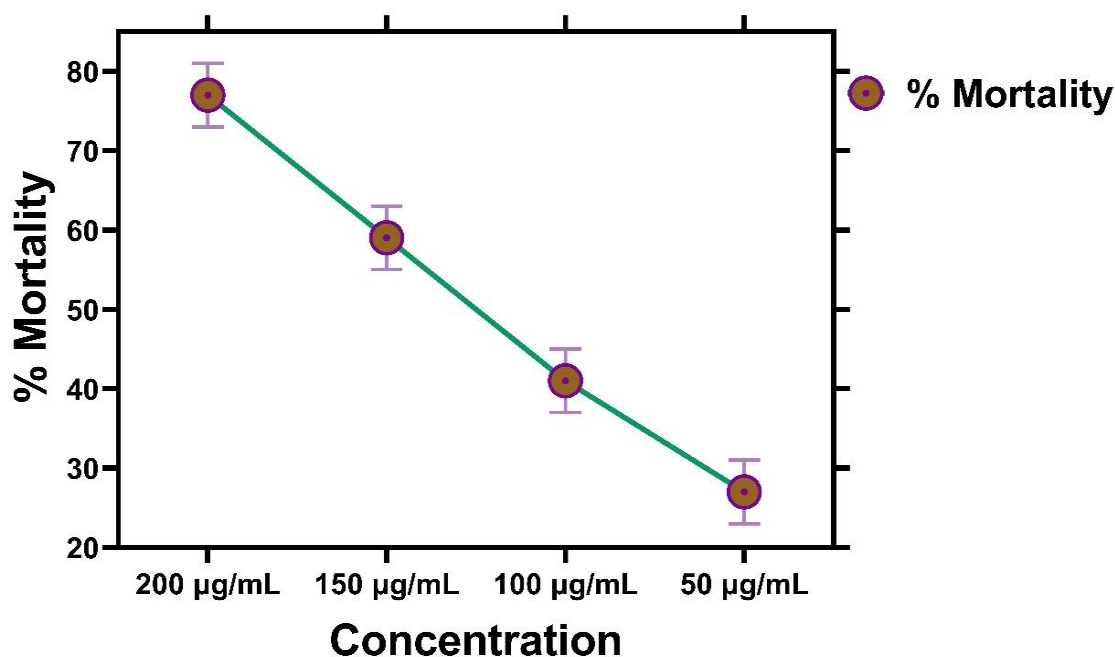


Figure 11. Cytotoxicity potential of IONPs against brine shrimp.

3. Materials and Methods

3.1. Chemicals

Various chemicals and catalysts that were used for this research were of scientific grade and were obtained from different chemical suppliers.

3.2. Collection and Preparation of Algal Extract

The blue-green algae *Oscillatoria limnetica* was collected from freshwater substrate of the district Mianwali Punjab, Pakistan, in March 2022. The algal sample was brought to the Algal Molecular Genetics Lab of Quaid-i-Azam University, Islamabad, Pakistan. The sample was streaked on the BG11 medium and placed in the growth chamber under yellow light. The authentic literature and a microscope were used for the identification of isolated strains [59,60]. After identification, the material was shade dried and then ground to obtain a fine powder. To obtain algal extract, 1 g of algal powder was mixed with 1 L of deionized water and boiled at 100 $^{\circ}\text{C}$ for 24 h [36]. Furthermore, Whatman filter paper was used to

filter the extract and was used for synthesis of NPs. The overall study outline has been summarized in Figure 12.

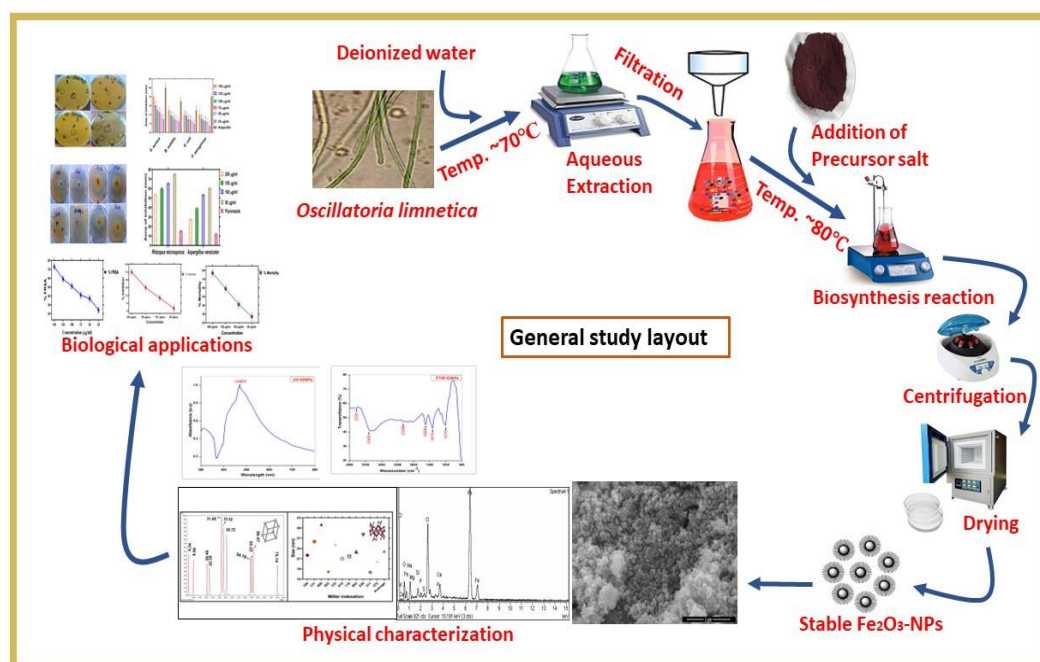


Figure 12. Detailed diagram showing green synthesis, characterization, and diverse biological application of IONPs.

3.3. Synthesis of IONPs

A standard protocol that was established by a previous study for the biosynthesis of IONPs was used with slight modifications [61]. To achieve this purpose, 1 Mm solution of Iron Chloride Hexahydrate ($\text{FeCl}_3 \cdot 6\text{H}_2\text{O}$) salt (Alfa Aesar, Haverhill, MA, USA) was added to algal extract, and 0.5 L of distilled water was mixed with 0.5 g of algal extract to synthesize iron NPs. On a hot plate, the mixed solution was kept with persistent stirring for 2 h at 80 °C. Initially, the formation of IONPs was determined by a change in color from light brown to dark brown. The solution was subjected to centrifugation at 12,000 rpm for 15 min to obtain pure IONPs. The supernatant was discarded, and the pellet was collected and then wiped with distilled water, followed by drying in an oven at 60 °C for 2 h. Furthermore, calcination was performed in an open-air furnace. Finally, dried IONPs were ground and stored at room temperature for further characterization to confirm their chemical composition and morphology.

3.4. Characterization of (IONPs)

3.4.1. UV-Visible Spectroscopy

Iron nanoparticle synthesis was performed by UV spectroscopy (UV-Vis 4000 spectrophotometer, Munich, Germany). The absorbance of iron NPs was evaluated at a wavelength ranging from 350 to 600 nm, and the wavelength of the peak was studied.

3.4.2. Fourier Transform Infrared Spectroscopy

The oscillatory properties were assessed using FTIR spectroscopy. The functional groups involved in stabilization and capping were identified using FTIR (Germany, Starnberg, Perkin Elmer Spectrum 65). The biosynthesized IONPs were coated onto KBr crystal wafers and then drained prior to measurements. The spectral range used to scan the sample was evaluated between 4000 and 500 cm^{-1} and assigned peak numbers.

3.4.3. X-ray Diffraction Analysis

The crystalline nature, size, and phase of IONPs were assessed using XRD. To study crystallographic description of purified IONPs, XRD pattern was evaluated using X-ray diffractive analysis (PANalytical, Eindhoven, The Netherlands) at a 45 kV voltage at 40 mA current. The sample was annealed Copper $K\alpha$ radiations with a silver monochromator between the 2θ range of $10\text{--}80^\circ$. Finally, the Debye–Scherer equation, $D = K \lambda / \beta_{1/2} \cos\theta$, was used to calculate size of NPs.

3.4.4. Scanning Electron Microscopy

Scanning electron microscopy was used to assess the morphology and particle size distribution of the sample. The morphological characters and size of IONPs were assessed using SEM (JSM5910, JEOL Tokyo, Japan) with voltages of 1 kV and 5 kV equipped with EDX detector.

3.4.5. Energy Dispersive X-ray Analysis

The composition of elements was studied using EDX. Fundamental analysis of iron nanoparticles was analyzed by an energy dispersive X-ray (EDX) detector.

3.5. Antibacterial Assay

Antibacterial assay of *Oscillatoria limnetica*-synthesized IONPs was determined through disc diffusion method [62] against different Gram-positive (*B. subtilis*, *S. aureus*) and Gram-negative (*E. coli*, *P. aeruginosa*) bacterial strains. Pure cultures of bacteria were subculture on nutrient agar media. Furthermore, each strain was washed onto different individual plates using sterile cotton swabs. Whatman filter paper was disinfected by autoclaving. For this purpose, 100 μL of bacterial strain was used to obtained bacterial lawns. After this, filter discs (5 mm) filled with 10 μL of test sample were loaded on bacterial lawn. In total, 10 μL of ampicillin disc was used as a positive control. Iron nanoparticle solution was loaded on each disc and were allowed to dry. Then, these dry discs were placed on inoculated agar media. Later, these petri plates were incubated at 37°C . After 24 h, the zone of inhibition was measured via vernier caliper. MIC values were determined in the concentration range of 150–25 $\mu\text{g}/\text{mL}$. Various stages of percentage inhibition of bacteria were measured by using the formula given below.

$$\% \text{ Inhibition} = [1 - (\text{Sample absorbance})/(\text{Absorbance of control})] \times 100$$

3.6. Antifungal Assay

The antifungal assay of IONPs was performed using different fungal strains (*Rhizopus microsporus* and *Aspergillus versicolor*). Preserved fungal cultures were refined on PDA media at 26°C for 7 days. The antifungal activity of iron nanoparticles was ascertained with the help of the poisoned food technique [63]. The PDA media was mixed with different concentration of IONPs in the range of 200–50 mg/mL . In the center of nanoparticle-amended PDA plates, cork borer was used to insert the 4 mm inoculum disc of the fungal strains. Petri plates were incubated at 26°C for 7 days. A chemical fungicide, Fluconazole, was used as a positive control. Percentage inhibition was measured according to the following formula.

$$\% \text{ Growth inhibition} = [(\text{Control} - \text{Treated})/(\text{Control})] \times 100$$

3.7. Antioxidant Assay

The antioxidant assay of iron nanoparticles was performed in terms of free radical activity using the DPPH assay [64]. The free radical scavenging assay was evaluated using different concentrations of IONPs ranging from 150 to 25 $\mu\text{g}/\text{mL}$. The DPPH solution was prepared at room temperature with 4 mg of 0.02 mM DPPH mixed in 100 mL of methanol. Ascorbic acid was taken as positive control, and DMSO was taken as a negative control.

Later, incubation was performed for 30 min, and readings were noted at 517 nm to evaluate the percent scavenging of DPPH using the following formula.

$$\% \text{FRSA} = [(Control \text{ Absorbance} - Sample \text{ absorbance}) / (Control \text{ absorbance})] \times 100$$

IC₅₀ was determined using a linear regression curve.

3.8. Hemolytic Assay

Biocompatibility against Human (RBCs)

Hemolytic activity was ascertained to evaluate the biocompatible nature of iron NPs with the aid of freshly extracted human RBCs [65]. To achieve this purpose, 2 mL of fresh human blood was collected and centrifuged at 15,000 rpm for 10 min. After this, plasma was removed, and 5 mL of 7.4 pH Phosphate Buffered Saline (PBS) was added, and the mixture was again centrifuged at 14,000 rpm for 5 min to remove the PBS residue. Then, 100 µL of blood was added to different concentrations of IONPs followed by incubation for 1 h at 35 °C, followed by centrifugation at 12,000 rpm for 15 min. The supernatant was transferred to a 96-well plate, and the reading was recorded at 530 nm to find the percent hemoglobin released. The PBS was used as a negative control, and Triton X-100 was used as the positive control. % Hemolysis was determined as follows.

$$\% \text{ Hemolysis} = [(Absorbance \text{ sample}) - (Absorbance \text{ of negative control}) / (Absorbance \text{ of positive control})] \times 100$$

3.9. Cytotoxicity Assay

Brine Shrimp Cytotoxicity Assay

Larvae of brine shrimp *Artemia salina* were used for the cytotoxicity assay to ascertain the in vitro cytotoxicity potential of IONPs [19]. *Artemia salina* eggs were incubated for 24–48 h under light at 30 °C in 1 L of sterile sea saltwater in a glass jar with continuous aeration. Once the larvae were hatched, active free floating nauplii were collected under light conditions and used for further analysis. Subsequently, 0.5 mL of iron NPs with different concentrations was transferred to the nauplii in each well. Vincristine sulphate was taken as the positive control, whereas DMSO was taken as the negative control. Under light conditions, each nauplii was transferred to different concentrations of iron NPs, respectively. The percentage of dead shrimps was determined in each well after incubation for 24 h, and the median lethality dose (LD₅₀) was calculated using GraphPad software.

4. Conclusions

Successful biosynthesis of crystalline hematite phase iron NPs has been synthesized using a novel, ecofriendly, and green synthesis protocol. Synthesized IONPs were extensively characterized using different techniques, such as UV, FTIR, XRD, SEM, and EDX. Our results explain effective biological properties of the iron NPs. Biosynthesized IONPs indicated potential in vitro biological activities such as antibacterial and antifungal activities. Furthermore, a moderate DPPH antioxidant assay was performed, and IONPs were found to be biocompatible using erythrocytes. Biosynthesized iron NPs were found to be minimally toxic to normal human RBCs. This study also hypothesized that the type of algal material can have important effects on its biomedical applications. In conclusion, our results showed that IONPs can be designed for different treatments. Moreover, we suggest further studies on the toxicity and biocompatibility aspects to further reveal their biosafe and biocompatible nature.

Author Contributions: M.H. and A.S.M. generated the idea. Supervision was provided by A.S.M. Experimental facilities were provided by A.S.M. Experimental study was performed by M.H. and J.I. M.H. wrote the manuscript. M.H., J.I., N.F., W.C. and M.T. helped with software, manuscript editing, and revision. M.A.E.-S. helped with manuscript editing, revision, and funding. All authors have read and agreed to the published version of the manuscript.

Funding: The authors would like to extend their sincere appreciation to the Researchers Supporting Project Number (RSP2023R182) King Saud University, Riyadh, Saudi Arabia.

Institutional Review Board Statement: Not applicable.

Informed Consent Statement: Informed consent was obtained from all subjects involved in the study.

Data Availability Statement: All the raw data of this research can be obtained from the corresponding authors upon reasonable request.

Conflicts of Interest: The authors declare no conflict of interest.

Sample Availability: Samples of the compounds are available from the authors.

References

1. Abbasi, B.A.; Iqbal, J.; Yaseen, T.; Zahra, S.A.; Ali, S.; Uddin, S.; Mahmood, T.; Kanwal, S.; El-Serehy, H.A.; Chalgham, W. Exploring Physical Characterization and Different Bio-Applications of *Elaeagnus angustifolia* Orchestrated Nickel Oxide Nanoparticles. *Molecules* **2023**, *28*, 654. [[CrossRef](#)] [[PubMed](#)]
2. Malik, S.B.; Saggu, J.I.; Gul, A.; Abbasi, B.A.; Iqbal, J.; Waris, S.; Jardan, Y.A.B.; Chalgham, W. Synthesis and characterization of silver and graphene nanocomposites and their antimicrobial and photocatalytic potentials. *Molecules* **2022**, *27*, 5184. [[CrossRef](#)] [[PubMed](#)]
3. Shousha, W.G.; Aboulthana, W.M.; Salama, A.H.; Saleh, M.H.; Essawy, E.A. Evaluation of the biological activity of Moringa oleifera leaves extract after incorporating silver nanoparticles, in vitro study. *Bull. Natl. Res. Cent.* **2019**, *43*, 212. [[CrossRef](#)]
4. Vasantharaj, S.; Sathiyavimal, S.; Saravanan, M.; Senthilkumar, P.; Gnanasekaran, K.; Shanmugavel, M.; Manikandan, E.; Pugazhendhi, A. Synthesis of ecofriendly copper oxide nanoparticles for fabrication over textile fabrics: Characterization of antibacterial activity and dye degradation potential. *J. Photochem. Photobiol. B Biol.* **2019**, *191*, 143–149. [[CrossRef](#)] [[PubMed](#)]
5. Xu, W.; Yang, T.; Liu, S.; Du, L.; Chen, Q.; Li, X.; Dong, J.; Zhang, Z.; Lu, S.; Gong, Y. Insights into the Synthesis, types and application of iron Nanoparticles: The overlooked significance of environmental effects. *Environ. Int.* **2022**, *158*, 106980. [[CrossRef](#)]
6. Uddin, S.; Iqbal, J.; Safdar, L.B.; Ahmad, S.; Abbasi, B.A.; Capasso, R.; Kazi, M.; Quraihi, U.M. Green synthesis of BPL-NiONPs using leaf extract of *Berberis pachyacantha*: Characterization and multiple in vitro biological applications. *Molecules* **2022**, *27*, 2064. [[CrossRef](#)]
7. Moraru, C.I.; Panchapakesan, C.P.; Huang, Q.; Takhistov, P.; Liu, S.; Kokini, J.L. Nanotechnology: A new frontier in food science understanding the special properties of materials of nanometer size will allow food scientists to design new, healthier, tastier, and safer foods. *Food Technol.* **2003**, *57*, 24–29.
8. Ullah, I.; Khalil, A.T.; Ali, M.; Iqbal, J.; Ali, W.; Alarifi, S.; Shinwari, Z.K. Green-synthesized silver nanoparticles induced apoptotic cell death in MCF-7 breast cancer cells by generating reactive oxygen species and activating caspase 3 and 9 enzyme activities. *Oxidative Med. Cell. Longev.* **2020**, *2020*, 1215395. [[CrossRef](#)]
9. Gopinath, V.; MubarakAli, D.; Priyadarshini, S.; Priyadharshini, N.M.; Thajuddin, N.; Velusamy, P. Biosynthesis of silver nanoparticles from *Tribulus terrestris* and its antimicrobial activity: A novel biological approach. *Colloids Surf. B Biointerfaces* **2012**, *96*, 69–74. [[CrossRef](#)]
10. Raghieb, F.; Naikoo, M.I.; Khan, F.A.; Alyemini, M.N.; Ahmad, P. Interaction of ZnO nanoparticle and AM fungi mitigates Pb toxicity in wheat by upregulating antioxidants and restricted uptake of Pb. *J. Biotechnol.* **2020**, *323*, 254–263. [[CrossRef](#)]
11. Mourdikoudis, S.; Pallares, R.M.; Thanh, N.T.K. Characterization techniques for nanoparticles: Comparison and complementarity upon studying nanoparticle properties. *Nanoscale* **2018**, *10*, 12871–12934. [[CrossRef](#)]
12. Abbasi, B.A.; Iqbal, J.; Israr, M.; Yaseen, T.; Zahra, S.A.; Shahbaz, A.; Rahdar, A.; Raouf, B.; Khan, S.U.; Kanwal, S.; et al. Rhamnella gilgitica functionalized green synthesis of ZnONPs and their multiple therapeutic properties. *Microsc. Res. Tech.* **2022**, *85*, 2338–2350. [[CrossRef](#)] [[PubMed](#)]
13. Christian, P.; Von der Kammer, F.; Baalousha, M.; Hofmann, T. Nanoparticles: Structure, properties, preparation and behaviour in environmental media. *Ecotoxicology* **2008**, *17*, 326–343. [[CrossRef](#)] [[PubMed](#)]
14. Shah, I.H.; Ashraf, M.; Sabir, I.A.; Manzoor, M.A.; Malik, M.S.; Gulzar, S.; Ashraf, F.; Iqbal, J.; Niu, Q.; Zhang, Y. Green synthesis and Characterization of Copper oxide nanoparticles using *Calotropis procera* leaf extract and their different biological potentials. *J. Mol. Struct.* **2022**, *1259*, 132696. [[CrossRef](#)]
15. Safat, S.; Buazar, F.; Albukhaty, S.; Matroodi, S. Enhanced sunlight photocatalytic activity and biosafety of marine-driven synthesized cerium oxide nanoparticles. *Sci. Rep.* **2021**, *11*, 14734. [[CrossRef](#)] [[PubMed](#)]
16. Hameed, S.; Khalil, A.T.; Ali, M.; Iqbal, J.; Rahman, L.; Numan, M.; Khamlich, S.; Maaza, M.; Ullah, I.; Abbasi, B.A.; et al. Precursor effects on the physical, biological, and catalytic properties of *Fagonia indica* Burm. f. mediated zinc oxide nanoparticles. *Microsc. Res. Tech.* **2021**, *84*, 3087–3103. [[CrossRef](#)] [[PubMed](#)]
17. Iqbal, J.; Abbasi, B.A.; Yaseen, T.; Zahra, S.A.; Shahbaz, A.; Shah, S.A.; Uddin, S.; Ma, X.; Raouf, B.; Kanwal, S. Green synthesis of zinc oxide nanoparticles using *Elaeagnus angustifolia* L. leaf extracts and their multiple in vitro biological applications. *Sci. Rep.* **2021**, *11*, 20988. [[CrossRef](#)] [[PubMed](#)]

18. Dahoumane, S.A.; Jeffryes, C.; Mechouet, M.; Agathos, S.N. Biosynthesis of inorganic nanoparticles: A fresh look at the control of shape, size and composition. *Bioengineering* **2017**, *4*, 14. [[CrossRef](#)]
19. Khalil, A.T.; Khan, M.D.; Razzaque, S.; Afridi, S.; Ullah, I.; Iqbal, J.; Tasneem, S.; Shah, A.; Shinwari, Z.K.; Revaprasadu, N. Single precursor-based synthesis of transition metal sulfide nanoparticles and evaluation of their antimicrobial, antioxidant and cytotoxic potentials. *Appl. Nanosci.* **2021**, *11*, 2489–2502. [[CrossRef](#)]
20. Uddin, S.; Safdar, L.B.; Iqbal, J.; Yaseen, T.; Laila, S.; Anwar, S.; Abbasi, B.A.; Saif, M.S.; Quraishi, U.M. Green synthesis of nickel oxide nanoparticles using leaf extract of *Berberis balochistanica*: Characterization, and diverse biological applications. *Microsc. Res. Tech.* **2021**, *84*, 2004–2016. [[CrossRef](#)]
21. Chouhan, C.; Rajput, R.P.S.; Sahu, R.; Verma, P.; Sahu, S. An updated review on nanoparticle based approach for nanogel drug delivery system. *J. Drug Deliv. Ther.* **2020**, *10*, 254–266. [[CrossRef](#)]
22. Hofmann, T.; Lowry, G.V.; Ghoshal, S.; Tufenkji, N.; Brambilla, D.; Dutcher, J.R.; Gilbertson, L.M.; Giraldo, J.P.; Kinsella, J.M.; Landry, M.P. Technology readiness and overcoming barriers to sustainably implement nanotechnology-enabled plant agriculture. *Nat. Food* **2020**, *1*, 416–425. [[CrossRef](#)]
23. Uddin, S.; Safdar, L.B.; Anwar, S.; Iqbal, J.; Laila, S.; Abbasi, B.A.; Saif, M.S.; Ali, M.; Rehman, A.; Basit, A. Green synthesis of nickel oxide nanoparticles from *Berberis balochistanica* stem for investigating bioactivities. *Molecules* **2021**, *26*, 1548. [[CrossRef](#)] [[PubMed](#)]
24. Shinde, S.; Folliero, V.; Chianese, A.; Zannella, C.; De Filippis, A.; Rosati, L.; Prisco, M.; Falanga, A.; Mali, A.; Galdiero, M. Synthesis of chitosan-coated silver nanoparticle bioconjugates and their antimicrobial activity against multidrug-resistant bacteria. *Appl. Sci.* **2021**, *11*, 9340. [[CrossRef](#)]
25. Shah, T.; Latif, S.; Saeed, F.; Ali, I.; Ullah, S.; Alsahli, A.A.; Jan, S.; Ahmad, P. Seed priming with titanium dioxide nanoparticles enhances seed vigor, leaf water status, and antioxidant enzyme activities in maize (*Zea mays* L.) under salinity stress. *J. King Saud Univ. Sci.* **2021**, *33*, 101207. [[CrossRef](#)]
26. Chang, S.-J.; Hsueh, T.-J.; Chen, I.-C.; Huang, B.-R. Highly sensitive ZnO nanowire CO sensors with the adsorption of Au nanoparticles. *Nanotechnology* **2008**, *19*, 175502. [[CrossRef](#)] [[PubMed](#)]
27. Ahmad, M.; Ali, A.; Ullah, Z.; Sher, H.; Dai, D.-Q.; Ali, M.; Iqbal, J.; Zahoor, M.; Ali, I. Biosynthesized silver nanoparticles using *Polygonatum geminiflorum* efficiently control fusarium wilt disease of tomato. *Front. Bioeng. Biotechnol.* **2022**, *10*, 1679. [[CrossRef](#)]
28. Lv, B.; Xu, Y.; Wu, D.; Sun, Y.J. Preparation of α -Fe₂O₃ nanodisks by blocking the growth of (001) plane. *J. Mater. Sci. Technol.* **2009**, *25*, 155.
29. Ahmad, P.; Alyemeni, M.N.; Al-Huqail, A.A.; Alqahtani, M.A.; Wijaya, L.; Ashraf, M.; Kaya, C.; Bajguz, A. Zinc oxide nanoparticles application alleviates arsenic (As) toxicity in soybean plants by restricting the uptake of as and modulating key biochemical attributes, antioxidant enzymes, ascorbate-glutathione cycle and glyoxalase system. *Plants* **2020**, *9*, 825. [[CrossRef](#)]
30. Ni, Y.; Ge, X.; Zhang, Z.; Ye, Q. Fabrication and characterization of the plate-shaped γ -Fe₂O₃ nanocrystals. *Chem. Mater.* **2002**, *14*, 1048–1052. [[CrossRef](#)]
31. Pereira, A.L.; Vasconcelos, V. Classification and phylogeny of the cyanobiont *Anabaena azollae* Strasburger: An answered question? *Int. J. Syst. Evol. Microbiol.* **2014**, *64*, 1830–1840. [[CrossRef](#)]
32. Rico, M.; González, A.G.; Santana-Casiano, M.; González-Dávila, M.; Pérez-Almeida, N.; de Tangil, M.S. Production of primary and secondary metabolites using algae. In *Prospects and Challenges in Algal Biotechnology*; Springer: Berlin/Heidelberg, Germany, 2017; pp. 311–326.
33. Ibrahim, H.; Reda, M.M.; Klingner, A. Preparation and characterization of green carboxymethylchitosan (CMCS)–Polyvinyl alcohol (PVA) electrospun nanofibers containing gold nanoparticles (AuNPs) and its potential use as biomaterials. *Int. J. Biol. Macromol.* **2020**, *151*, 821–829. [[CrossRef](#)] [[PubMed](#)]
34. Iqbal, J.; Abbasi, B.A.; Ahmad, R.; Shahbaz, A.; Zahra, S.A.; Kanwal, S.; Munir, A.; Rabbani, A.; Mahmood, T. Biogenic synthesis of green and cost effective iron nanoparticles and evaluation of their potential biomedical properties. *J. Mol. Struct.* **2020**, *1199*, 126979. [[CrossRef](#)]
35. Abdel-Raouf, N.; Al-Enazi, N.M.; Ibraheem, I.B.M.; Alharbi, R.M.; Alkhulaifi, M.M. Biosynthesis of silver nanoparticles by using of the marine brown alga *Padina pavonia* and their characterization. *Saudi J. Biol. Sci.* **2019**, *26*, 1207–1215. [[CrossRef](#)]
36. Thema, F.; Manikandan, E.; Dhlamini, M.; Maaza, M. Green synthesis of ZnO nanoparticles via *Agathosma betulina* natural extract. *Mater. Lett.* **2015**, *161*, 124–127. [[CrossRef](#)]
37. Iqbal, J.; Abbasi, B.A.; Mahmood, T.; Hameed, S.; Munir, A.; Kanwal, S. Green synthesis and characterizations of Nickel oxide nanoparticles using leaf extract of *Rhamnus virgata* and their potential biological applications. *Appl. Organomet. Chem.* **2019**, *33*, e4950. [[CrossRef](#)]
38. Salem, D.M.; Ismail, M.M.; Tadros, H.R. Evaluation of the antibiofilm activity of three seaweed species and their biosynthesized iron oxide nanoparticles (Fe₃O₄-NPs). *Egypt. J. Aquat. Res.* **2020**, *46*, 333–339. [[CrossRef](#)]
39. Sarkar, R.; Kumbhakar, P.; Mitra, A. Green synthesis of silver nanoparticles and its optical properties. *Dig. J. Nanomater. Biostructures* **2010**, *5*, 491–496.
40. Al-Radadi, N.S.; Hussain, T.; Faisal, S.; Shah, S.A.R. Novel biosynthesis, characterization and bio-catalytic potential of green algae (*Spirogyra hyalina*) mediated silver nanomaterials. *Saudi J. Biol. Sci.* **2022**, *29*, 411–419.

41. Mahanty, S.; Bakshi, M.; Ghosh, S.; Chatterjee, S.; Bhattacharyya, S.; Das, P.; Das, S.; Chaudhuri, P. Green synthesis of iron oxide nanoparticles mediated by filamentous fungi isolated from Sundarban mangrove ecosystem, India. *Bionanoscience* **2019**, *9*, 637–651. [[CrossRef](#)]
42. Shankar, S.; Rhim, J.-W. Amino acid mediated synthesis of silver nanoparticles and preparation of antimicrobial agar/silver nanoparticles composite films. *Carbohydr. Polym.* **2015**, *130*, 353–363. [[CrossRef](#)] [[PubMed](#)]
43. Menazea, A.; Ahmed, M. Silver and copper oxide nanoparticles-decorated graphene oxide via pulsed laser ablation technique: Preparation, characterization, and photoactivated antibacterial activity. *Nano-Struct. Nano-Objects* **2020**, *22*, 100464. [[CrossRef](#)]
44. Orr, J.C.; Fabry, V.J.; Aumont, O.; Bopp, L.; Doney, S.C.; Feely, R.A.; Gnanadesikan, A.; Gruber, N.; Ishida, A.; Joos, F. Anthropogenic ocean acidification over the twenty-first century and its impact on calcifying organisms. *Nature* **2005**, *437*, 681–686. [[CrossRef](#)] [[PubMed](#)]
45. Mikhailova, E.O. Silver nanoparticles: Mechanism of action and probable bio-application. *J. Funct. Biomater.* **2020**, *11*, 84. [[CrossRef](#)]
46. Liu, C.; Ginn, H.M.; Dejnirattisai, W.; Supasa, P.; Wang, B.; Tuekprakhon, A.; Nutalai, R.; Zhou, D.; Mentzer, A.J.; Zhao, Y. Reduced neutralization of SARS-CoV-2 B. 1.617 by vaccine and convalescent serum. *Cell* **2021**, *184*, 4220–4236.e4213. [[CrossRef](#)] [[PubMed](#)]
47. Qiu, Y.; Wu, Y.; Lu, B.; Zhu, G.; Gong, T.; Wang, R.; Peng, Q.; Li, Y. Inhibition of methicillin-resistant *Staphylococcus aureus* (MRSA) biofilm by cationic poly (D, L-lactide-co-glycolide) nanoparticles. *J. Bioadhesion Biofilm Res.* **2020**, *36*, 159–168. [[CrossRef](#)] [[PubMed](#)]
48. Singh, A.; Gautam, P.K.; Verma, A.; Singh, V.; Shivapriya, P.M.; Shivalkar, S.; Sahoo, A.K.; Samanta, S.K. Green synthesis of metallic nanoparticles as effective alternatives to treat antibiotics resistant bacterial infections: A review. *Biotechnol. Rep.* **2020**, *25*, e00427. [[CrossRef](#)]
49. Mohamed, H.E.A.; Afridi, S.; Khalil, A.T.; Ali, M.; Zohra, T.; Salman, M.; Ikram, A.; Shinwari, Z.K.; Maaza, M. Bio-redox potential of *Hyphaene thebaica* in bio-fabrication of ultrafine maghemite phase iron oxide nanoparticles (Fe₂O₃ NPs) for therapeutic applications. *Mater. Sci. Eng. C* **2020**, *112*, 110890. [[CrossRef](#)]
50. Antony, V.S.; Silky, V.; Raji, P.; SaiPriya, C.; Selvarani, J.A. Bioactivity Studies of *Datura metel*, *Aegle marmelos*, *Annona reticulata* and *Saraca indica* and their Green Synthesized Silver Nanoparticle. *J. Pure Appl. Microbiol.* **2019**, *13*, 329–338.
51. Cao, Y.; Wang, J.; Jian, F.; Xiao, T.; Song, W.; Yisimayi, A.; Huang, W.; Li, Q.; Wang, P.; An, R. Omicron escapes the majority of existing SARS-CoV-2 neutralizing antibodies. *Nature* **2022**, *602*, 657–663. [[CrossRef](#)]
52. Khalil, A.T.; Ovais, M.; Ullah, I.; Ali, M.; Shinwari, Z.K.; Maaza, M. Biosynthesis of iron oxide (Fe₂O₃) nanoparticles via aqueous extracts of *Sageretia thea* (Osbeck.) and their pharmacognostic properties. *Green Chem. Lett. Rev.* **2017**, *10*, 186–201. [[CrossRef](#)]
53. Khalil, I.; Yehye, W.A.; Etxeberria, A.E.; Alhadi, A.A.; Dezfooli, S.M.; Julkapli, N.B.M.; Basirun, W.J.; Seyfoddin, A. Nanoantioxidants: Recent trends in antioxidant delivery applications. *Antioxidants* **2019**, *9*, 24. [[CrossRef](#)]
54. Dobrovolskaia, M.A.; McNeil, S.E. Understanding the correlation between in vitro and in vivo immunotoxicity tests for nanomedicines. *J. Control. Release* **2013**, *172*, 456–466. [[CrossRef](#)] [[PubMed](#)]
55. Raguvaran, R.; Manuja, A.; Manuja, B.K. Zinc oxide nanoparticles: Opportunities and challenges in veterinary sciences. *Immunome Res.* **2015**, *11*, 1.
56. Sankarganesh, P.; Ganesh Kumar, A.; Parthasarathy, V.; Joseph, B.; Priyadharsini, G.; Anbarasan, R.J. Synthesis of *Murraya koenigii* Mediated Silver Nanoparticles and Their In Vitro and In Vivo Biological Potential. *J. Inorg. Organomet. Polym. Mater.* **2021**, *31*, 2971–2979. [[CrossRef](#)]
57. Ullah, M.O.; Haque, M.; Urmi, K.F.; Zulfiker, A.H.M.; Anita, E.S.; Begum, M.; Hamid, K. Anti-bacterial activity and brine shrimp lethality bioassay of methanolic extracts of fourteen different edible vegetables from Bangladesh. *Asian Pac. J. Trop. Biomed.* **2013**, *3*, 1–7. [[CrossRef](#)]
58. Kumar, P.; Selvi, S.S.; Praba, A.; Selvaraj, M.; Rani, L.M.; Suganthi, P.; Devi, B.S.; Govindaraju, M. Antibacterial activity and in-vitro cytotoxicity assay against brine shrimp using silver nanoparticles synthesized from *Sargassum ilicifolium*. *Dig. J. Nanomater. Biostructures* **2012**, *7*, 1447–1455.
59. Cohen, Y.; Padan, E.; Shilo, M.J. Facultative anoxygenic photosynthesis in the cyanobacterium *Oscillatoria limnetica*. *J. Bacteriol.* **1975**, *123*, 855–861. [[CrossRef](#)]
60. Hassan, D.; Khalil, A.T.; Saleem, J.; Diallo, A.; Khamlich, S.; Shinwari, Z.K.; Maaza, M. Biosynthesis of pure hematite phase magnetic iron oxide nanoparticles using floral extracts of *Callistemon viminalis* (bottlebrush): Their physical properties and novel biological applications. *Artif. Cells Nanomed. Biotechnol.* **2018**, *46*, 693–707. [[CrossRef](#)]
61. Kiani, B.H.; Haq, I.-U.; Alhodaib, A.; Basheer, S.; Fatima, H.; Naz, I.; Ur-Rehman, T. Comparative Evaluation of Biomedical Applications of Zinc Nanoparticles Synthesized by Using *Withania somnifera* Plant Extracts. *Plants* **2022**, *11*, 1525. [[CrossRef](#)]
62. Ali, M.; Haroon, U.; Khizar, M.; Chaudhary, H.J.; Munis, M.F.H. Scanning electron microscopy of bio-fabricated Fe₂O₃ nanoparticles and their application to control brown rot of citrus. *Microsc. Res. Tech.* **2021**, *84*, 101–110. [[CrossRef](#)]
63. Ali, M.; Haroon, U.; Khizar, M.; Chaudhary, H.J.; Munis, M.F.H. Facile single step preparations of phyto-nanoparticles of iron in *Calotropis procera* leaf extract to evaluate their antifungal potential against *Alternaria alternata*. *Curr. Plant Biol.* **2020**, *23*, 100157. [[CrossRef](#)]

64. Hassan, D.; Khalil, A.T.; Solangi, A.R.; El-Mallul, A.; Shinwari, Z.K.; Maaza, M. Physiochemical properties and novel biological applications of *Callistemon viminalis*-mediated α -Cr₂O₃ nanoparticles. *Appl. Organometal. Chem.* **2019**, *33*, e5041. [[CrossRef](#)]
65. Khalil, A.T.; Ovais, M.; Ullah, I.; Ali, M.; Shinwari, Z.K.; Hassan, D.; Maaza, M. *Sageretia thea* (Osbeck.) modulated biosynthesis of NiO nanoparticles and their in vitro pharmacognostic, antioxidant and cytotoxic potential. *Artif. Cells Nanomed. Biotechnol.* **2018**, *46*, 838–852. [[CrossRef](#)] [[PubMed](#)]

Disclaimer/Publisher's Note: The statements, opinions and data contained in all publications are solely those of the individual author(s) and contributor(s) and not of MDPI and/or the editor(s). MDPI and/or the editor(s) disclaim responsibility for any injury to people or property resulting from any ideas, methods, instructions or products referred to in the content.